

Attribute-Aware Deep Hashing with Self-Consistency for Large-Scale Fine-Grained Image Retrieval

Xiu-Shen Wei, *Member, IEEE*, Yang Shen, Xuhao Sun, Peng Wang, *Member, IEEE*, Yuxin Peng, *Senior Member, IEEE*

Abstract—Our work focuses on tackling large-scale fine-grained image retrieval as ranking the images depicting the concept of interests (*i.e.*, the same sub-category labels) highest based on the fine-grained details in the query. It is desirable to alleviate the challenges of both fine-grained nature of small inter-class variations with large intra-class variations and explosive growth of fine-grained data for such a practical task. In this paper, we propose attribute-aware hashing networks with self-consistency for generating attribute-aware hash codes to not only make the retrieval process efficient, but also establish explicit correspondences between hash codes and visual attributes. Specifically, based on the captured visual representations by attention, we develop an encoder-decoder structure network of a reconstruction task to unsupervisedly distill high-level attribute-specific vectors from the appearance-specific visual representations without attribute annotations. Our models are also equipped with a feature decorrelation constraint upon these attribute vectors to strengthen their representative abilities. Then, driven by preserving original entities' similarity, the required hash codes can be generated from these attribute-specific vectors and thus become attribute-aware. Furthermore, to combat simplicity bias in deep hashing, we consider the model design from the perspective of the self-consistency principle and propose to further enhance models' self-consistency by equipping an additional image reconstruction path. Comprehensive quantitative experiments under diverse empirical settings on six fine-grained retrieval datasets and two generic retrieval datasets show the superiority of our models over competing methods. Moreover, qualitative results demonstrate that not only the obtained hash codes can strongly correspond to certain kinds of crucial properties of fine-grained objects, but also our self-consistency designs can effectively overcome simplicity bias in fine-grained hashing.

Index Terms—Large-Scale Fine-Grained Image Retrieval; Learning-to-Hash; Attribute-Aware; Simplicity Bias; Self-Consistency.



1 INTRODUCTION

FINE-grained image retrieval [1] in computer vision and pattern recognition aims to retrieve images belonging to multiple subordinate categories of a super-category (*aka* a meta-category), *e.g.*, different species of animals/plants [2], different models of cars [3], different kinds of retail products [4], etc. Its key challenge therefore lies in understanding fine-grained visual differences that subtly distinguish objects that are highly similar in overall appearance, but differ in *fine-grained* features. Also, fine-grained retrieval still demands ranking all the instances so that images depicting the same sub-category label are ranked highest based on the fine-grained details in the query.

In particular, with the explosive growth of fine-grained data in real applications [2], [4], [5], [6], [7], fine-grained hashing, as a promising solution for dealing with large-scale fine-grained retrieval tasks, has proven to be able to greatly reduce the storage cost and increase the query speed [8], [9] benefiting from the learned compact binary hash code representations. While previous work, *e.g.*, [8], [9], achieved good retrieval performance, however, the hash codes they generated lack semantic correspondence, *i.e.*, they did not capture *fine-grained attributes*. These attributes, such as head colors, tail colors, male, female, living habits, are as effective descriptions of fine-grained objects, that can be understood by both humans and computers. In this paper, to establish an explicit correspondence between hash codes and visual attributes to simultaneously improve large-scale fine-grained retrieval accuracy and integrate interpretation into deep learning based hash methods, we propose unified Attribute-Aware hashing Networks, termed as A²-NET and A²-NET⁺⁺, for achieving these goals (cf. Figure 1).

In both A²-NET and A²-NET⁺⁺, considering huge labor cost of supervised attribute annotations, we adopt an unsupervised setting to automatically capture discriminative visual attributes from still images and then associate the learned hash code representations to these attributes. Therefore, a hash bit of learned hash codes could be both discriminative and interpretable. Additionally, thanks to the unsupervised setting, the attributes derived from our models will be not restricted to pre-defined attributes like

- X.-S. Wei is with School of Computer Science and Engineering, and Key Laboratory of New Generation Artificial Intelligence Technology and Its Interdisciplinary Applications, Southeast University, China. Y. Shen and X. Sun are with School of Computer Science and Engineering, Nanjing University of Science and Technology, China. P. Wang is with School of Computer Science and Engineering, University of Electronic Science and Technology of China, China. Y. Peng is with Wangxuan Institute of Computer Technology, and National Key Laboratory for Multimedia Information Processing, Peking University, China. Y. Peng is the corresponding author.
- This work was supported by National Key R&D Program of China (2021YFA1001100), National Natural Science Foundation of China under Grants (62272231, 62132001, 61925201), Natural Science Foundation of Jiangsu Province of China under Grant (BK20210340), the Fundamental Research Funds for the Central Universities (No. NJ2022028), and CAAI-Huawei MindSpore Open Fund.

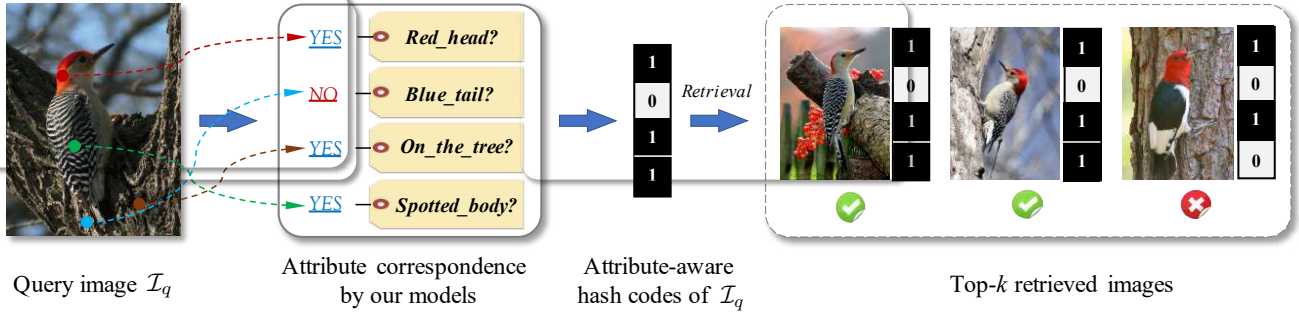


Figure 1. Key idea of our models, as well as the main process of fine-grained hashing based on our *attribute-aware* hash codes. Concretely, regarding a query image \mathcal{I}_q of Red bellied Woodpecker, after returning all the correct results, a fine-grained image belonging to Red headed Woodpecker closest to the query image in terms of Hamming distance is also retrieved.

supervised-based attribute learning methods [10], [11], [12], [13]. Moreover, it can distill the most useful properties of fine-grained objects as attribute-aware hash codes in such an end-to-end trainable manner for accurate retrieval among multiple similar subordinate categories.

More specifically, as the overall framework shown in Figure 2, our A^2 -NET, as the base model w.r.t. A^2 -NET⁺⁺, consists of a fine-grained representation learning module and an attribute-aware hash codes generation module. It first leverages attention mechanisms to model fine-grained patterns in terms of both global-level deep features T_i and local-level cues T_i^c from input image \mathcal{I}_i . Then, the appearance-specific features of these visual patterns T are aggregated and translated into semantic-specific representations x_i . After that, we formulate the aforementioned unsupervised attribute learning as a reconstruction task of projecting x_i to an attribute vector v_i by performing an encoder-decoder structure network. Therefore, it can be expected that in the high-level attribute space, v_i could correspond to certain kinds of nameable properties of fine-grained objects. Moreover, a feature decorrelation constraint is further introduced upon v_i to both enhance the discriminative ability and remove the redundancy among these dimensions of attribute-specific features. Finally, our attribute-aware hash codes u_i are generated from v_i by conducting the hash code learning procedure.

It is noticed that the most crucial mechanism to generate the attribute-aware internal latent representations of inputs is the encoder-decoder structure in our proposal. It realizes a reconstruction paradigm by reconstructing the holistic feature representation x_i . Beyond acquiring the implicit representations, we also find that such a structure explicitly conforms to the principle of self-consistency [14] in deep networks. The self-consistency principle encourages an intelligent system to seek a most self-consistent model for observations of the external world by minimizing the internal discrepancy between the observed and the regenerated, which enables the system to learn as comprehensive information as possible that is sensed. Therefore, to verify the merits of our proposal, we conduct preliminary experiments on a constructed dataset, *i.e.*, *MNIST-CIFAR* [15]. This special dataset consists of images by vertically concatenating *MNIST* [16] images onto *CIFAR-10* [17] images, with ten classes where each class is a combination of a unique *MNIST* class and *CIFAR-10* class. After networks training converges on this dataset, we

can visualize the learned activations on the *MNIST-CIFAR* images to show whether there is more attention on complex patterns comparing to the *CIFAR* parts or more attention on simple patterns comparing to the *MNIST* parts. As expected, it is clear that, our proposal, which exhibits self-consistency, attends to more complex and comprehensive patterns than the vanilla baseline. More importantly, these observations validate the simplicity bias phenomenon [15] of networks in deep hash learning for the first time to our best knowledge. Detailed preliminary findings and discussions can refer to Section 3.4.

Therefore, to overcome the simplicity bias and then improve the retrieval accuracy, we propose to further enhance the self-consistency in our models. Specifically, we realize this idea by equipping an additional simple but effective path upon the basic A^2 -NET, where the original input image \mathcal{I}_i is required to be reconstructed. Such a model with both reconstruction features and images as its necessary functions can more faithfully reflect self-consistency, thereby alleviating simplicity bias and achieving better hash retrieval accuracy, which is thus termed as the advanced A^2 -NET⁺⁺ model.

To evaluate our models, we conduct extensive experiments on five fine-grained retrieval benchmark datasets, *i.e.*, *CUB200-2011* [18], *Aircraft* [19], *Food101* [20], *NABirds* [21] and *VegFru* [7], for validating the effectiveness and on two generic image datasets, *i.e.*, *NUS-WIDE* [22] and *COCO* [23], for investigating the universality. Additionally, two challenging empirical settings, *i.e.*, zero-shot fine-grained retrieval on three aforementioned fine-grained datasets and cross-domain fine-grained retrieval on the *Clothing* dataset [10], are also incorporated in comparisons for proving the generalization ability, as well as the models' robustness. Quantitative results of retrieval accuracy on these datasets and settings show that our proposed models obviously and consistently outperform existing state-of-the-art methods. Also, the ablation studies of these crucial components in our models validate their own effectiveness. In particular, to evaluate the attribute-aware retrieval performance, which is regarded as one of the most important characteristics of our models, we perform both qualitative analyses and quantitative attribute matching to demonstrate that our learned hash bits have strong correspondences to visual attributes of fine-grained objects, even without employing attribute supervisions or part-level annotations. In addition, more visualization results of simplicity bias on these fine-grained retrieval datasets are

presented, which demonstrate that our models are able to effectively alleviate simplicity bias for fine-grained hashing.

Note that a preliminary version of this paper was published as a conference paper (Spotlight Presentation) [24] in *Advances in Neural Information Processing Systems 2021*. In this journal paper, we have made significant extensions. First, we systematically investigate the simplicity bias [15] problem in deep hashing, and provide in-depth discussions from the self-consistency principle [14] perspective. Second, we propose an advanced model, *i.e.*, A^2 -NET⁺⁺, which not only achieves much better fine-grained hashing retrieval accuracy but also confirms the conjecture about the advantage of the self-consistency design in our models. Third, we conduct more comprehensive experiments and analyses to evaluate our models from many diverse aspects, such as effectiveness, robustness, generalization ability, interpretation, etc.

The rest of the paper is organized as follows. Section 2 retrospects the related work. Section 3 introduces the details of our proposed models, as well as the investigation about simplicity bias in deep hashing. Experiments and analyses of both qualitative and quantitative aspects are provided in Section 4. Section 5 presents conclusions and future work.

2 RELATED WORK

We briefly review the related work in the following four aspects, *i.e.*, fine-grained image retrieval, learning to hash, the studies about visual attributes in computer vision problems, and simplicity bias in deep neural networks.

2.1 Fine-Grained Image Retrieval

Fine-grained image retrieval as an integral part of fine-grained image analysis [1] has gained more and more traction in recent years [8], [24], [25], [26], [27], [28], [29], [30]. What makes it challenging is that objects of fine-grained images have only subtle differences, and often largely vary in pose, scale, and orientation or can exhibit cross-modal differences (*e.g.*, sketch-based retrieval [28]).

Depending on the type of query image, the most studied areas of fine-grained image retrieval can be separated into two groups: fine-grained content-based image retrieval (FG-CBIR) and fine-grained sketch-based image retrieval (FG-SBIR). More specifically, in FG-CBIR, unsupervised learning based [25] and supervised learning based methods [26], [27], [31] were developed from different perspectives for handling fine-grained retrieval tasks, *e.g.*, localizing fine-grained parts [25], enhancing intra-class separability with inter-class compactness [27], and reducing the confidence of the fine-grained predictions [31], etc. While, FG-SBIR needs to not only capture fine-grained characteristics present in the sketches, but also possess the ability to traverse the sketch and image domain gap. In the literature of FG-SBIR, the earlier work, *e.g.*, [29], [32], [33], were mostly based on Siamese-triplet networks [34] to tackle the aforementioned challenges. Recently, some work tried to incorporate the advances of recent progress in self-supervised learning [35] and attention mechanisms [36] for further improving the retrieval accuracy of FG-SBIR, *e.g.*, [30], [37].

However, although these fine-grained retrieval methods achieved good results, they still have the limitations in the

face of large-scale data, *i.e.*, the searching time for the exact nearest neighbor is typically expensive or even impossible for the given queries. To alleviate this issue, fine-grained hashing, which aims to generate compact binary codes to represent fine-grained images, as a promising direction has attracted the attention in the fine-grained community very recently [8], [38], [39]. More specifically, ExchNet [8] was the first to define the fine-grained hashing task and develop a fine-grained tailored method to firstly locate discriminative object parts and further learn binary hash codes for representing fine-grained images. In the same period, DSaH [38] was proposed to automatically mine salient regions and learn semantic-preserving hash codes simultaneously. Recently, FISH [39] was developed with a double-filtering mechanism and a proxy-based loss function for handling fine-grained hashing. Unfortunately, the learned hash bits of these methods lack any semantics which are more meaningful to fine-grained objects, and thus lack the model interpretability. Compared with them, our models can not only outperform previous fine-grained hashing methods, but more importantly, the learned hash codes of our models are *attribute-aware*, *i.e.*, our hash bits have strong correspondence to semantic visual properties that are useful for fine-grained image retrieval.

2.2 Learning to Hash

Hashing [40] is a widely-studied solution to approximate nearest neighbor search, which transforms the data item to a short code consisting of a sequence of bits (*i.e.*, hash codes). The research efforts of hashing can be categorized into two groups, including data-independent hashing (*aka* locality sensitive hashing [41], [42], [43]) and data-dependent hashing (*aka* learning to hash [44], [45], [46], [47], [48], [49]).

Specifically, locality sensitive hashing methods attempted to adjust hash learning from different perspectives, *e.g.*, the theory or machine learning views, to name a few: proposing random hash functions satisfying local sensitive property [41], developing better search schemes [42], providing faster computation of hash functions [43], etc. While, compared with locality sensitive hashing methods, since data-dependent hashing methods learn hash functions from a specific dataset to achieve similarity preserving, they can generally obtain superior retrieval accuracy. Especially for capitalizing on advances in deep learning, many well-performing methods were proposed to integrate feature learning and hash code learning into an end-to-end framework based on deep networks, *e.g.*, [44], [45], [46], [48], [49]. In particular, very recently researchers in the vision community have begun to pay attention to the more challenging and practical hashing task, *i.e.*, fine-grained hashing [8], [38], [39]. Distant from these previous work, our proposed models equip these learned hash codes with strong correspondence to visual attributes, and meanwhile are able to combat simplicity bias [15] with our self-consistency designs for dealing with large-scale fine-grained image retrieval.

2.3 Visual Attributes

Attributes are typically mid-level semantic properties of objects [50], such as colors (*e.g.*, “red”, “blue”), texture (*e.g.*, “striped”, “spotted”), or even life habits of animals (*e.g.*, “living on the tree”, “living in the water”). Visual

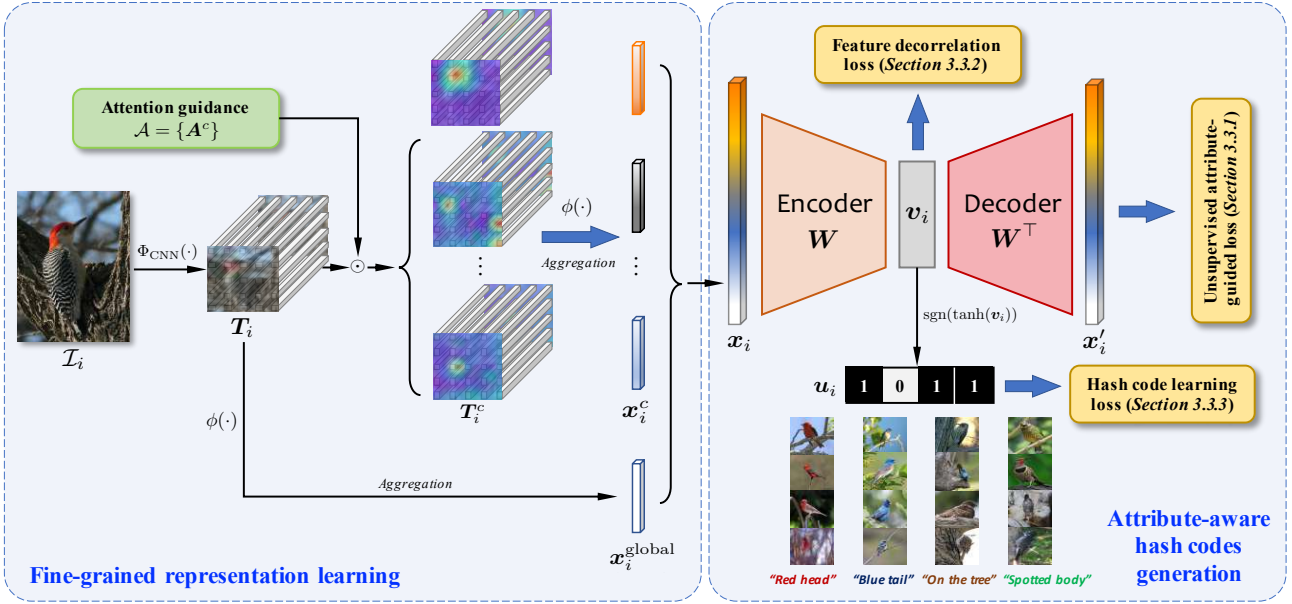


Figure 2. Overall framework of the basic A²-NET model, which consists of two crucial modules, *i.e.*, fine-grained representation learning and attribute-aware hash codes generation. The whole network can be end-to-end trainable, and is generally driven by the unsupervised attribute-guided reconstruction loss, the feature decorrelation loss and the hash code learning loss, cf. Section 3.3.

attributes have exhibited their impact for strengthening various vision tasks, including facial verification [11], fine-grained categorization [12], zero-shot transfer [13], scene understanding [51], and so on. Most of the previous attribute learning methods are supervised by costly human-generated annotations and also are dependent on pre-defined attribute labels, *e.g.*, [10], [11], [12], [13]. In consequence, for large-scale problems, these supervised methods might be not feasible due to the restriction caused by the cumbersome obtained attribute annotations. Moreover, even for some tasks, their visual attributes are quite hard to define. In this paper, to alleviate the aforementioned issues, we propose the A²-NET and A²-NET⁺⁺ models to formulate an *unsupervised learning* structure to project the learned visual features into an attribute space where it finally generates attribute-aware binary hash codes. Compared with previous attribute learning methods, our models are independent with pre-defined attribute labels, and could automatically learn discriminative attribute-aware hash codes in a unified end-to-end trainable fashion. Furthermore, our models can not only correspond hash bits to visual attributes tailored for fine-grained objects, which shows significant improvements of retrieval accuracy, but also offer an intuitive way of deep hashing interpretation.

2.4 Simplicity Bias in Neural Networks

Simplicity bias (SB) refers to the inherent tendency of human perception and cognition to favor simple and easily interpretable explanations or representations over complex ones. In the literature of machine learning, SB, *i.e.*, the tendency of supervised neural networks to find simple patterns, was proposed to analyze the generalization of neural networks [15], [52]. In particular, in [15], it originally showed that neural networks trained with stochastic gradient descent are biased to learning the simplest predictive features in the data, while overlooking the complex but equally-predictive

patterns. Inspired by this, Teney *et al.* [53] demonstrated that SB can be mitigated through a diversity constraint and explored how to improve out of distribution generalization by overcoming SB.

In the context of fine-grained image retrieval, SB can play a significant role in shaping our perception and interpretation of detailed visual information. Fine-grained image retrieval deals with the retrieval tasks of objects or entities within a specific category that exhibit subtle and intricate visual differences. These differences may be challenging to discern and require careful examination of fine details. However, SB leads us to overlook or underestimate the importance of these fine-grained details. Our cognitive inclination towards simplicity may push us towards making more general and coarse classifications, focusing on prominent features or easily distinguishable patterns while neglecting the nuances and subtle variations that are essential for accurate fine-grained retrieval. In this paper, to our best knowledge, we are the first to investigate the SB problem in the fine-grained image retrieval task, and propose methods from the model’s self-consistency perspective [14] to effectively mitigate SB in fine-grained image-oriented hash code learning.

3 METHODOLOGY

In this section, we introduce the overall framework, notations of the proposed models, as well as elaborating its crucial modules and the enhanced self-consistency designs for further alleviating the simplicity bias.

3.1 Overall Framework and Notations

As illustrated in Figure 2, our basic A²-NET model consists of two crucial modules, *i.e.*, a fine-grained representation learning module and an attribute-aware hash codes generation module. Given an input image \mathcal{I}_i , based on its

corresponding deep activation tensor $\mathbf{T}_i \in \mathbb{R}^{C \times H \times W}$ extracted by a backbone CNN, a set of attention guidance $\mathcal{A} = \{\mathbf{A}^c\}$ is learned for capturing fine-grained tailored local patterns \mathbf{T}_i^c from \mathbf{T}_i . To distill semantical cues and further generate the final attribute-aware binary hash codes, we propose to transform these appearance-specific features \mathbf{T} towards semantic-specific representations $\hat{\mathbf{T}}$ by performing a transform network $\phi(\cdot)$. After aggregating $\hat{\mathbf{T}}$, the obtained attentive local-level features \mathbf{x}_i^c are associated with the global-level feature $\mathbf{x}_i^{\text{global}}$ to form as a holistic feature representation \mathbf{x}_i . In order to generate attribute-aware binary hash codes, we conduct a reconstruction paradigm to project \mathbf{x}_i as \mathbf{v}_i in an attribute space where its data point corresponds to an attribute vector w.r.t. a certain kind of nameable properties of fine-grained objects (e.g., “red head” or “spotted body”). Furthermore, with the aid of feature decorrelation, \mathbf{v}_i is expected to be more discriminative by removing redundant correlation information. Finally, hash code learning is performed upon \mathbf{v}_i to obtain the final attribute-aware binary codes \mathbf{u}_i .

3.2 Fine-Grained Representation Learning

Attention plays an important role in human perception [36], [54], and humans exploit a sequence of partial glimpses and selectively focus on salient parts of an object or a scene in order to better capture visual structure [55]. Inspired by this, we incorporate the attention mechanism into representation learning to capture fine-grained local patterns for distinguishing subtle differences between these subordinate categories.

Concretely, we extract the deep feature of its input image \mathcal{I}_i via a backbone CNN model $\Phi_{\text{CNN}}(\cdot)$ by

$$\mathbf{T}_i = \Phi_{\text{CNN}}(\mathcal{I}_i) \in \mathbb{R}^{C \times H \times W}. \quad (1)$$

Then, based on \mathbf{T}_i , multiple attention guidances ($\mathbf{A}^c \in \mathbb{R}^{H \times W}$) are generated as a set of attention maps, i.e., \mathcal{A} . The attention guidance \mathbf{A}^c is designed to evaluate which deep descriptors [25] in these $H \times W$ cells should be attended or even overlooked by conducting

$$\mathbf{T}_i^c = \mathbf{A}^c \odot \mathbf{T}_i, \quad (2)$$

where \odot is the element-wise Hadamard product. To obtain the final attribute-aware binary codes, it is desirable to transform these appearance-specific (i.e., low-level) features \mathbf{T} to semantic-specific (i.e., mid-level) representations which are closer to the attribute space. Thus, a transforming network $\phi(\cdot)$, which is equipped with a stack of convolution layers, is performed on \mathbf{T} as follows:

$$\hat{\mathbf{T}}_i^c = \phi(\mathbf{T}_i^c; \theta_{\text{local}}), \quad (3)$$

$$\hat{\mathbf{T}}_i = \phi(\mathbf{T}_i; \theta_{\text{global}}), \quad (4)$$

where θ presents the parameters of the corresponding transforming networks w.r.t. \mathbf{T}_i^c and \mathbf{T}_i , respectively. Then, we aggregate $\hat{\mathbf{T}}_i^c$ and $\hat{\mathbf{T}}_i$ by conducting global average-pooling and correspondingly obtain the attentive local-level features \mathbf{x}_i^c , as well as the global-level feature $\mathbf{x}_i^{\text{global}}$. The holistic feature representation w.r.t. the input image \mathcal{I}_i is achieved by concatenating both \mathbf{x}_i^c and $\mathbf{x}_i^{\text{global}}$, i.e., $\mathbf{x}_i = [\mathbf{x}_i^c; \mathbf{x}_i^{\text{global}}] = F(\mathcal{I}_i; \Theta) \in \mathbb{R}^d$. Note that, we hereby

abstract the aforementioned fine-grained feature learning process as a function $F(\mathcal{I}_i; \Theta)$ associated with parameters Θ .

3.3 Attribute-Aware Hash Codes Generation

How to generate attribute-aware hash codes is the key of our A²-NET model. We elaborate it in the following three aspects, i.e., unsupervised attribute-guided learning, attribute-specific feature decorrelation, and hash code learning.

3.3.1 Unsupervised Attribute-Guided Learning

In real-applications, especially for the large-scale and fine-grained tasks, attribute annotations are always infeasible, which limits the learning process to be conducted in an unsupervised setting. While, in the literature, the main goal of unsupervised learning is to capture regularities in data for the purpose of extracting useful representations or for restoring corrupted data [56]. Many unsupervised methods explicitly produce *internal latent units or codes*, from which the data is to be reconstructed.

Inspired by this, we develop an unsupervised attribute-guided reconstruction component to project the holistic representation \mathbf{x}_i of \mathcal{I}_i into a latent space, i.e., the attribute space \mathcal{V} . In \mathcal{V} , its high-level vectors are designed to have certain desirable properties, e.g., corresponding to semantic properties of fine-grained objects (*aka* “fine-grained attributes”).

More specifically, in our A²-NET, the unsupervised attribute-guided learning is realized by a reconstruction paradigm with an encoder-decoder structure, as shown in Figure 2. Concretely, given a batch of n training data \mathcal{I}_i , their holistic representations $\mathbf{X} = \{\mathbf{x}_1; \mathbf{x}_2; \dots; \mathbf{x}_n\} \in \mathbb{R}^{d \times n}$ can be obtained as aforementioned. By formulation, the encoder projects \mathbf{X} into the attribute space \mathcal{V} with a projection matrix $\mathbf{W} \in \mathbb{R}^{k \times d}$ to get an internal latent representation $\mathbf{V} \in \mathbb{R}^{k \times n}$ w.r.t. \mathbf{X} . In particularly, we set that the dimension of latent representation k equals the number of hash bits in the final binary hash code \mathbf{u}_i . Furthermore, each column of \mathbf{V} , i.e., $\mathbf{v}_i \in \mathbb{R}^k$, can derive \mathbf{u}_i by

$$\mathbf{u}_i = \text{sgn}(\tanh(\mathbf{v}_i)). \quad (5)$$

Meanwhile, regarding \mathbf{v}_i , we also consider to reconstruct its input \mathbf{x}_i by a decoder as a counterpart of the encoder. Therefore, on one hand, such a reconstruction paradigm can reduce and further distill high-level semantic cues in the attribute space \mathcal{V} . While, on the other hand, it can drive the training of A²-NET by preserving the similarity between queried hash codes and database points in terms of hash code learning (cf. Section 3.3.3).

Concretely, the learning objective of unsupervised attribute-guided reconstruction is written as follows:

$$\min_{\mathbf{W}} \|\mathbf{X} - \mathbf{W}^{\top} \mathbf{W} \mathbf{X}\|_F^2 \quad \text{s.t.} \quad \mathbf{W} \mathbf{X} = \mathbf{V}' = \tanh(\mathbf{V}), \quad (6)$$

where the decoder (i.e., a counterpart of the encoder) is realized by \mathbf{W}^{\top} to simplify the network. However, directly minimizing Eq. (6) with a hard constraint is difficult to optimize. Therefore, we relax the constraint into a soft constraint, and the learning objective can be rewritten as

$$\min_{\mathbf{W}} \|\mathbf{X} - \mathbf{W}^{\top} \mathbf{V}'\|_F^2 + \lambda \|\mathbf{W} \mathbf{X} - \mathbf{V}'\|_F^2. \quad (7)$$

3.3.2 Attribute-Specific Feature Decorrelation

By conducting the aforementioned unsupervised attribute-guided learning, we can obtain the internal latent vectors \mathbf{V}' as the attribute-specific features. In order to both enhance the discriminative ability and remove the redundant correlation among these attribute-specific features, we introduce a feature decorrelation constraint upon \mathbf{V}' , which is formulated by

$$\min_{\mathbf{V}'} \|\mathbf{V}'\mathbf{V}'^\top - n\mathbf{I}\|_F^2, \quad (8)$$

where \mathbf{I} is the identity matrix and n is the batch size. Such a feature decorrelation constraint is preferable to construct independent features and reduce redundant information. Therefore, based on both unsupervised attribute-guided reconstruction and attribute-specific feature decorrelation, the final learned hash codes are expected to be both attribute-aware and hash-bit independent.

3.3.3 Hash Code Learning

In the following, we conduct the hash code learning based on the obtained attribute-specific features. Assume that we have n query data points which are denoted as $\{\mathbf{q}_i\}_{i=1}^n$, as well as m database points which are denoted as $\{\mathbf{v}_j\}_{j=1}^m$. Note that, both \mathbf{q}_i and \mathbf{v}_j are belonging to the attribute space \mathcal{V} . By following Eq. (5), the corresponding binary hash codes can be obtained via

$$\mathbf{u}_i = \text{sgn}(\tanh(\mathbf{q}_i)), \quad (9)$$

$$\mathbf{z}_j = \text{sgn}(\tanh(\mathbf{v}_j)), \quad (10)$$

where $\mathbf{u}_i, \mathbf{z}_j \in \{-1, +1\}^k$. The goal of our hash code learning is to learn binary hash codes for both query points and database points from $\{\mathbf{q}_i\}_{i=1}^n, \{\mathbf{v}_j\}_{j=1}^m$, and the pairwise supervised information, *i.e.*, $\mathbf{S} \in \{-1, +1\}^{n \times m}$. To preserve the pairwise similarity, we adopt the ℓ_2 loss between the supervised information (*aka* similarity) and the inner product of query-database point binary code pairs. It can be formulated as follows:

$$\begin{aligned} & \min_{\mathbf{U}, \mathbf{Z}} \sum_{i=1}^n \sum_{j=1}^m (\mathbf{u}_i^\top \mathbf{z}_j - kS_{ij})^2 \\ \text{s.t. } & \mathbf{U} \in \{-1, +1\}^{n \times k}, \mathbf{Z} \in \{-1, +1\}^{m \times k}, \end{aligned} \quad (11)$$

where S_{ij} is the pairwise similarity label in \mathbf{S} .

Overall, we get the final objective of the A²-NET model by considering Eq. (7), Eq. (8) and Eq. (11) together as follows:

$$\begin{aligned} \min_{\mathbf{W}, \Theta} \mathcal{L}(\mathcal{I}) = & \|\mathbf{X} - \mathbf{W}^\top \mathbf{V}'\|_F^2 + \lambda \|\mathbf{W}\mathbf{X} - \mathbf{V}'\|_F^2 \\ & + \alpha \|\mathbf{V}'\mathbf{V}'^\top - n\mathbf{I}\|_F^2 + \beta \sum_{i=1}^n \sum_{j=1}^m (\mathbf{u}_i^\top \mathbf{z}_j - kS_{ij})^2, \end{aligned} \quad (12)$$

where λ, α and β are hyper-parameters as the trade-off.

In practice, during training, it might be only available a set of database points $\{\mathbf{v}_j\}_{j=1}^m$ without query points. Thus, we randomly sample n data points from database to construct a query set, and denote the indices of all the database points as Γ with the indices of the query set as Ω . Additionally, because we cannot back-propagate the gradient to Θ due to the $\text{sgn}(\cdot)$ function, we omit the $\text{sgn}(\cdot)$ function and only apply $\tanh(\cdot)$ for relaxation in Eq. (10) of the whole optimization process. Therefore, the optimization

formulation of A²-NET can be rewritten with only database points $\{\mathbf{v}_j\}_{j=1}^m$ for training as:

$$\begin{aligned} \min_{\mathbf{W}, \Theta} \mathcal{L}(\mathcal{I}) = & \|\mathbf{X} - \mathbf{W}^\top \mathbf{V}'\|_F^2 + \lambda \|\mathbf{W}\mathbf{X} - \mathbf{V}'\|_F^2 \\ & + \alpha \|\mathbf{V}'\mathbf{V}'^\top - n\mathbf{I}\|_F^2 \\ & + \beta \sum_{i \in \Omega} \sum_{j \in \Gamma} \left(\tanh(\mathbf{W} \cdot F(\mathcal{I}_i; \Theta))^\top \mathbf{z}_j - kS_{ij} \right)^2. \end{aligned} \quad (13)$$

For optimization, our A²-NET does not require complicated two-stage learning algorithms, *e.g.*, the alternative optimization strategy. In experiments, we employ the back-propagation algorithm and follow [46] to train the whole A²-NET model in a unified end-to-end manner.

3.4 Enhancing Model's Self-Consistency

When obtaining attribute-aware internal latent representations of the input images, we employ an encoder-decoder structure as a reconstruction paradigm. Beyond acquiring the implicit representations, such a structure is actually an explicit manifestation of the principle of *self-consistency* [14].

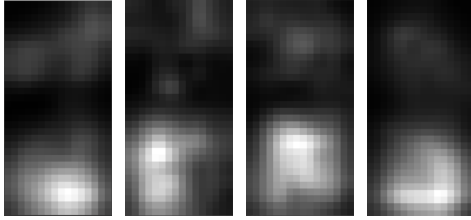
The self-consistency principle [14] encourages that an autonomous intelligent system seeks a most self-consistent model for observations of the external world by minimizing the internal discrepancy between the observed and the regenerated. That is to say, the intelligent system should be able to regenerate the distribution of the observed data from the compressed representation to the point that itself cannot distinguish internally despite its best effort. In the contrary, as a consequence, we conjecture that, in the absence of self-consistency, the model will exhibit a tendency to simplicity bias [15], [53] according to the information bottleneck framework [57], [58], [59] in deep neural networks.

3.4.1 Preliminary Empirical Studies of Simplicity Bias on Deep Hashing

Simplicity bias (SB) [15] is recently observed from neural networks trained with stochastic gradient descent, which shows the networks rely preferentially on few simple predictive features while ignoring more complex predictive features. The SB phenomenon partially explains the lack of robustness and generalization of deep neural networks in various vision problems, *e.g.*, out of distribution [53], confidence calibration [60], etc. In order to validate and explicitly observe the simplicity bias on deep hashing, we hereby firstly conduct a series of preliminary experiments.

Concretely, we follow the MNIST-CIFAR dataset introduced in [15] to perform deep hashing. More specifically, each image of the MNIST-CIFAR dataset is constructed by vertically concatenating MNIST [16] images onto CIFAR-10 [17] images. The dataset contains 10 classes, where each class is a combination of a unique MNIST class and CIFAR-10 class, cf. Figure 3. It is apparent to see that the MNIST part contains much simpler patterns than the CIFAR part.

In our preliminary experiments, we employ the ResNet-32 [61] model as the backbone. Thus, the baseline model is ResNet-32 by equipping with a vanilla learning-to-hash loss to keep the pairwise similarity (cf. Eqn. (11)), which is denoted as "BASELINE". We also follow the training/test splits in [15] to train both BASELINE and our A²-NET. Until

Figure 3. Examples of the *MNIST-CIFAR* dataset [15].

(a) Activations by BASELINE

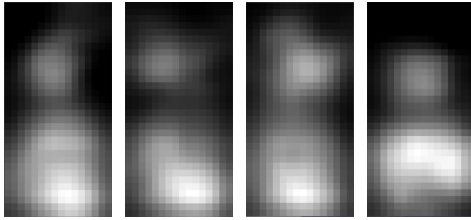
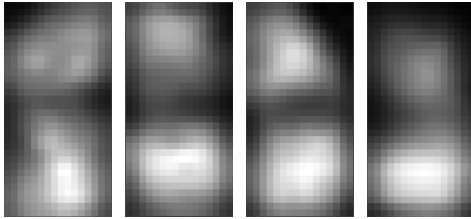
(b) Activations by our A^2 -NET(c) Activations by our A^2 -NET⁺⁺

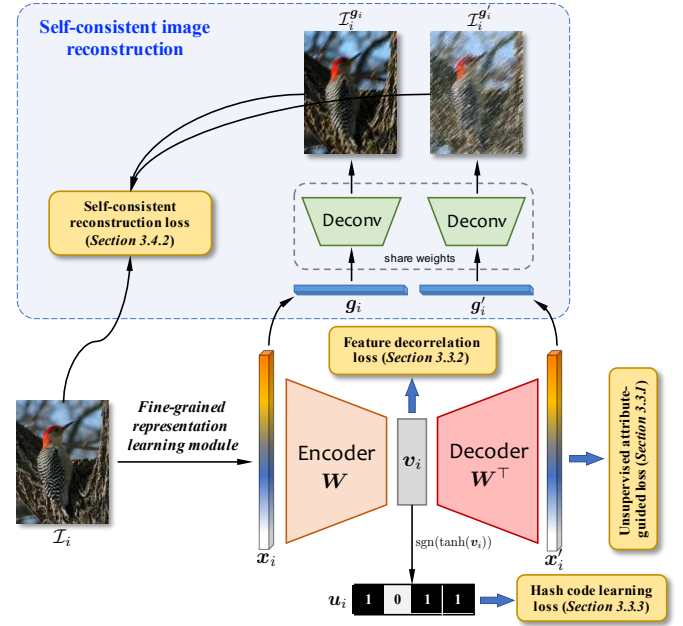
Figure 4. Activations obtained by BASELINE with vanilla hashing losses and our proposed models with self-consistency designs.

models convergence, we visualize the activations of input *MNIST-CIFAR* images in the test set (also Figure 3). As the activations shown in Figure 4a, it can be clearly observe that, for BASELINE, the *MNIST* parts are activated while the *CIFAR* parts are partially or nearly completely ignored. This observation indicates SB indeed happens in deep hashing because in this dataset digit patterns of *MNIST* are simpler than the object patterns of *CIFAR*.

To further inspect the SB in deep hashing quantitatively, we leave the training data of *MNIST-CIFAR* intact, while proposing different setups of test data, *i.e.*, *MNIST-CIFAR*, *MNIST-only*, and *CIFAR-only*. *MNIST-only/CIFAR-only* means that we only use the *MNIST/CIFAR* part for test. The results are reported in the column of BASELINE in Table 1. As presented, compared with the testing accuracy on *MNIST-CIFAR*, retrieval accuracy on *MNIST-only* has a slight drop, as the network focused mainly on the *MNIST* part. However, the test data of *CIFAR-only* shows a large overall accuracy reduction, which confirms the existence of SB in deep hash learning again.

Table 1
Preliminary results of retrieval accuracy (% mAP) on the *MNIST-CIFAR* dataset.

Test data	# bits	BASELINE	A^2 -NET	A^2 -NET ⁺⁺
<i>MNIST-CIFAR</i>	12	99.69	99.70	99.70
	24	99.68	99.71	99.73
	32	99.71	99.71	99.72
	48	99.73	99.74	99.75
<i>MNIST-only</i>	12	99.55	99.58	99.52
	24	99.60	99.64	99.59
	32	99.36	99.37	99.32
	48	99.52	99.52	99.51
<i>CIFAR-only</i>	12	21.05	21.23	24.50
	24	21.33	22.06	25.67
	32	21.66	22.67	26.40
	48	21.33	23.54	29.40

Figure 5. Illustration of the advanced A^2 -NET⁺⁺ model, which has an additional self-consistent image reconstruction modules over A^2 -NET, and can still be trained in an end-to-end manner.

On the other side, regarding the results of our A^2 -NET, we can find that our model alleviates the SB issue from both qualitative and quantitative aspects. Specifically, as shown in Figure 4b, the activations of A^2 -NET on the *CIFAR* part are significantly enhanced. Meanwhile, the retrieval accuracy of A^2 -NET on *CIFAR-only* also obtains consistent improvements for all the different lengths of hash codes.

3.4.2 Advanced A^2 -NET⁺⁺ Model

Combined with the preliminary empirical results and the self-consistency principle argument in [14], [57], we basically confirm our conjecture about the advantage of our encoder-decoder reconstruction structure in A^2 -NET. To further alleviate the simplicity bias and then improve the retrieval accuracy, we aim to enhance the model's self-consistency and propose the advanced A^2 -NET⁺⁺ model.

In fact, a more natural way to realize self-consistency is to reconstruct the original image representation \mathcal{I}_i itself, rather than reconstructing the holistic feature representation \mathbf{x}_i . It could

be expected to encourage more comprehensive features to combat with the simplicity bias in deep hashing. Motivated by this, we add two additional reconstructions over \mathcal{I}_i on the basic A²-NET, which is detailedly illustrated in Figure 5.

More specifically, based on $\mathbf{x}_i \in \mathbb{R}^d$, we first obtain a more compact feature $\mathbf{g}_i \in \mathbb{R}^{d'}$ by performing $\mathbf{W}'\mathbf{x}_i$, where $\mathbf{W}' \in \mathbb{R}^{d' \times d}$ is a linear transformation and $d' \ll d$. Then, a deconvolutional network [62] $\Psi_{\text{Deconv}}(\cdot; \Pi)$ is applied upon \mathbf{g}_i , which is expected to reconstruct the input raw image \mathcal{I}_i with its parameter Π . We denote the reconstructed output w.r.t. \mathbf{g}_i as $\mathcal{I}_i^{\mathbf{g}_i}$. In the similar way, we can also get the reconstructed $\mathcal{I}_i^{\mathbf{g}'_i}$ derived from \mathbf{g}'_i w.r.t. \mathbf{x}'_i . Regarding $\mathcal{I}_i^{\mathbf{g}_i}$ and $\mathcal{I}_i^{\mathbf{g}'_i}$, we minimize the internal discrepancy between their input \mathcal{I}_i and themselves by performing a self-consistent reconstruction loss, which is as follows.

$$\begin{aligned} & \min_{\mathbf{W}', \Pi} \|\mathcal{I}_i^{\mathbf{g}_i} - \mathcal{I}_i\|_F^2 + \|\mathcal{I}_i^{\mathbf{g}'_i} - \mathcal{I}_i\|_F^2 \\ &= \min_{\mathbf{W}', \Pi} \|\Psi_{\text{Deconv}}(\mathbf{g}_i; \Pi) - \mathcal{I}_i\|_F^2 + \|\Psi_{\text{Deconv}}(\mathbf{g}'_i; \Pi) - \mathcal{I}_i\|_F^2 \\ &= \min_{\mathbf{W}', \Pi} \|\Psi_{\text{Deconv}}(\mathbf{W}'\mathbf{x}_i; \Pi) - \mathcal{I}_i\|_F^2 \\ & \quad + \|\Psi_{\text{Deconv}}(\mathbf{W}'\mathbf{x}'_i; \Pi) - \mathcal{I}_i\|_F^2. \end{aligned} \quad (14)$$

Such a dual reconstruction structure of \mathbf{g}_i and \mathbf{g}'_i is actually to better enhance the self-consistency nature of the model, while also better constraining the intermediate features, *e.g.*, \mathbf{x}_i and \mathbf{x}'_i , learned in the previous modules.

Therefore, by incorporating Eq. (13), the final learning objective of our advanced A²-NET⁺⁺ model is formulated as:

$$\begin{aligned} \min_{\mathbf{W}, \Theta, \mathbf{W}', \Pi} \mathcal{L}(\mathcal{I}) &= \|\mathbf{X} - \mathbf{W}^\top \mathbf{V}'\|_F^2 + \lambda \|\mathbf{W}\mathbf{X} - \mathbf{V}'\|_F^2 \\ & \quad + \alpha \|\mathbf{V}'\mathbf{V}'^\top - n\mathbf{I}\|_F^2 \\ & \quad + \beta \sum_{i \in \Omega} \sum_{j \in \Gamma} \left(\tanh(\mathbf{W} \cdot F(\mathcal{I}_i; \Theta))^\top \mathbf{z}_j - kS_{ij} \right)^2 \\ & \quad + \eta \|\Psi_{\text{Deconv}}(\mathbf{W}'\mathbf{x}_i; \Pi) - \mathcal{I}_i\|_F^2 \\ & \quad + \eta \|\Psi_{\text{Deconv}}(\mathbf{W}'\mathbf{x}'_i; \Pi) - \mathcal{I}_i\|_F^2, \end{aligned} \quad (15)$$

where η is the trade-off parameter of the enhanced self-consistent reconstruction losses. It notes that, enhancing models's self-consistency for A²-NET⁺⁺ does not affect the ease of end-to-end training of A²-NET.

Additionally, we apply A²-NET⁺⁺ on the MNIST-CIFAR dataset to continue the preliminary experiments, and show the qualitative visualization and quantitative results in Figure 4c and Table 1, respectively. It is clearly to find that A²-NET⁺⁺ can further combat simplicity bias based on its enhanced self-consistency design (cf. Figure 5).

3.5 Out-of-Sample Extension

After training, our learned model can be applied for generating binary codes for query points including unseen query points in the training phase. Specifically, we can use the following equation to generate the binary code for \mathcal{I}_q :

$$\mathbf{u}_q = \text{sgn}(\tanh(\mathbf{W} \cdot F(\mathcal{I}_q; \Theta))). \quad (16)$$

4 EXPERIMENTS

In this section, we present the implementation details, empirical settings, main results, ablation studies and also

some interesting qualitative analyses of the learned attribute-aware binary hash codes.

4.1 Datasets

Beyond evaluating the retrieval accuracy on fine-grained image retrieval tasks on fine-grained benchmarks, we further involve generic image retrieval datasets for comparisons to justify the effectiveness of our models.

4.1.1 Fine-Grained Image Retrieval Datasets

We conduct experiments on five fine-grained benchmark datasets, *i.e.*, CUB200-2011 [18], Aircraft [19], Food101 [20], NABirds [21] and VegFru [7]. Specifically, CUB200-2011 is one of the most popular fine-grained datasets. It contains 11,788 bird images from 200 bird species and is officially split into 5,994 images for training and 5,794 images for test. Aircraft contains 10,000 images spanning 100 aircraft models with 3,334 for training, 3,333 for validation and 3,333 for test. For large-scale datasets, Food101 contains 101 kinds of food with 101,000 images, where for each class, 250 test images are checked manually for correctness while 750 training images still contain a certain amount of noises. NABirds has 48,562 images of North American birds with 555 sub-categories, where 23,929 for training and 24,633 for test. VegFru is another large-scale fine-grained dataset covering 200 kinds of vegetables and 92 kinds of fruit with 29,200 for training, 14,600 for validation and 116,931 for test.

Furthermore, the Clothing dataset [10] is also used for evaluating fine-grained retrieval accuracy in the cross-domain scenario, as well as quantitatively performing comparisons in terms of attribute-level matching for our attribute-aware models. This dataset consists of cross-scenario image pairs of online shopping images and corresponding offline user photos with fine-grained clothing attributes. The number of online images is about 450,000 with additional 90,000 offline counterparts collected. Each image has about 5-9 semantic attribute categories, with more than a hundred possible attribute values. The training and test splits in our experiments are followed [10].

4.1.2 Generic Image Retrieval Datasets

NUS-WIDE [22] and COCO [23] are two popular generic image benchmark datasets, which are employed as test beds for generic image retrieval evaluation. Concretely, NUS-WIDE [22] consists of 269,648 web images associated with tags. It is a multi-label dataset where each image might be annotated with multi-labels. We choose images from the 21 most frequent categories for evaluation by following [44], [46]. COCO [23] is another multi-label dataset, containing 82,783 training, 40,504 validation images which belong to 91 categories. For the training image set, we discard the images which have no category information. Following the protocols of these datasets in generic deep hashing [44], [45], [46], two images will be defined as a ground-truth neighbor (similar pair) if they share at least one common label.

4.2 Comparison Methods and Implementation Details

We hereby introduce the comparison methods and implementation details of our models.

Table 2

Comparisons of retrieval accuracy (% mAP) on five fine-grained benchmark datasets. For fair comparisons, the backbone of these methods in this table is ResNet-50. Best results are marked in bold.

Datasets	# bits	ITQ	SDH	DPSH	HashNet	ADSH	ExchNet	A ² -NET	A ² -NET ⁺⁺
<i>CUB200-2011</i>	12	6.80	10.52	8.68	12.03	20.03	25.14	33.83	37.83
	24	9.42	16.95	12.51	17.77	50.33	58.98	61.01	71.73
	32	11.19	20.43	12.74	19.93	61.68	67.74	71.61	78.39
	48	12.45	22.23	15.58	22.13	65.43	71.05	77.33	82.71
<i>Aircraft</i>	12	4.38	4.89	8.74	14.91	15.54	33.27	40.00	57.53
	24	5.28	6.36	10.87	17.75	23.09	45.83	63.66	73.45
	32	5.82	6.90	13.54	19.42	30.37	51.83	72.51	81.59
	48	6.05	7.65	13.94	20.32	50.65	59.05	81.37	86.65
<i>Food101</i>	12	6.46	10.21	11.82	24.42	35.64	45.63	46.44	54.51
	24	8.20	11.44	13.05	34.48	40.93	55.48	66.87	81.46
	32	9.70	13.36	16.41	35.90	42.89	56.39	74.27	82.92
	48	10.07	15.55	20.06	39.65	48.81	64.19	82.13	83.66
<i>NABirds</i>	12	2.53	3.10	2.17	2.34	2.53	5.22	8.20	8.80
	24	4.22	6.72	4.08	3.29	8.23	15.69	19.15	22.65
	32	5.38	8.86	3.61	4.52	14.71	21.94	24.41	29.79
	48	6.10	10.38	3.20	4.97	25.34	34.81	35.64	42.94
<i>VegFru</i>	12	3.05	5.92	6.33	3.70	8.24	23.55	25.52	30.54
	24	5.51	11.55	9.05	6.24	24.90	35.93	44.73	60.56
	32	7.48	14.55	10.28	7.83	36.53	48.27	52.75	73.38
	48	8.74	16.45	9.11	10.29	55.15	69.30	69.77	82.80

4.2.1 Comparison Methods

In experiments of fine-grained hashing, we compare our proposed models to the following competitive hashing methods, *i.e.*, ITQ [63], SDH [47], DPSH [64], HashNet [65], and ADSH [46]. Among them, DPSH, HashNet and ADSH are deep learning based methods. Furthermore, we also compare the results of our A²-NET and A²-NET⁺⁺ with state-of-the-arts of fine-grained hashing methods, including ExchNet [8]. Additionally, other fine-grained hashing methods, *i.e.*, DSaH [38] and FISH [39], also achieved good retrieval accuracy. However, as their empirical settings are different from other mainstream fine-grained hashing methods, for fair comparisons, we strictly control empirical settings the same as those of [38] and [39] and compare the results of our models with their results in the appendices.

For the comparisons of generic hashing, we further involve two recent state-of-the-art methods, *i.e.*, CSQ [44] and OrthoCos+BN [45], in experiments on the *NUS-WIDE* and *COCO* generic image retrieval datasets.

4.2.2 Implementation Details

For fair comparisons of fine-grained hashing, we follow the efficient training setting in ExchNet [8]. Concretely, for *CUB200-2011*, *Aircraft* and *Food101*, we sample 2,000 images per epoch, while 4,000 samples are randomly selected for *NABirds*, *VegFru* and *Clothing*. For the training details, regarding the backbone model, we can choose any network structure as the base network for the fine-grained representation learning module. Following [8], ResNet-50 [61] is employed in experiments. For generic hashing, 4,000 samples are randomly selected for *NUS-WIDE* and *COCO*. The backbone model employs the CNN-F model [66] by following [46].

For *CUB200-2011*, *Aircraft*, *Food101*, *NABirds* and *VegFru*, we follow [8] to perform such settings upon our proposed models. The total number of training epochs is 20, and the

number of batch size is set as 16. Different from [8], our model only requires a smaller iteration number to converge. Specifically, for these datasets containing less than 20,000 training images, the iteration number T_{\max} is 60, and the learning rate is divided by 10 at the 50th iteration. For other datasets, T_{\max} is set as 70, and the learning rate is divided by 10 at the 60th iteration.

For *NUS-WIDE*, *COCO* and *Clothing*, we adopt the training settings from [46], [67]. Concretely, regarding *NUS-WIDE* and *COCO*, the total number of training epochs is 3, and T_{\max} is set as 50. Regarding *Clothing*, the total number of training epochs is 10, and T_{\max} is set as 15. The number of batch size for these three datasets is set as 16. The learning rate is 10^{-4} .

For all datasets, the image resolution is 224×224 . The optimizer of our models is standard mini-batch stochastic gradient descent with the weight decay as 10^{-4} . The number of attention guidance equals the number of hash bits. The value of d' in A²-NET⁺⁺ is set to 1024. The hyper-parameters, *i.e.*, λ , α and β in Eq. (15), are set as 1 , $\frac{1}{n \times k}$ and $\frac{12}{k}$, respectively. The value of η is 0.5 for the *MNIST-CIFAR* dataset, while being 0.1 for other datasets.

4.3 Main Results

We present the main results from the following five aspects: 1) On fine-grained image datasets for validating the effectiveness; 2) On generic image datasets for investigating the universality; 3) In zero-shot fine-grained retrieval setting for proving the generalization ability; 4) In cross-domain fine-grained retrieval setting for justifying the robustness; and 5) Time and space complexity during inference.

4.3.1 Comparisons on Fine-Grained Image Datasets

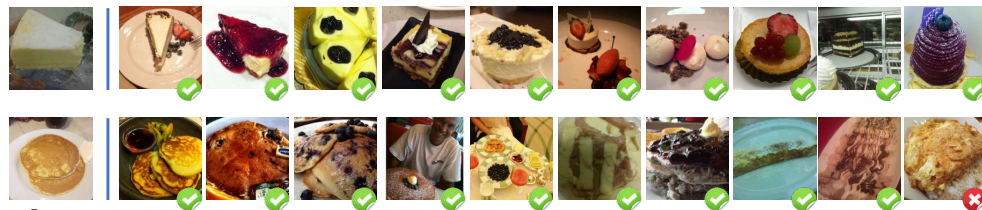
Table 2 presents the mean average precision (mAP) results of fine-grained retrieval on these five aforementioned fine-grained benchmark datasets. For each dataset, we report



Top-10 retrieved images

(a) *CUB200-2011*

Top-10 retrieved images

(b) *Aircraft*

Top-10 retrieved images

(c) *Food101*

Top-10 retrieved images

(d) *NABirds*

Top-10 retrieved images

(e) *VegFru*

Top-10 retrieved images

(f) *Clothing*Figure 6. Examples of top-10 retrieved images on six fine-grained datasets of 48-bit hash codes by our A²-NET++.

Table 3

Comparisons of retrieval accuracy (% mAP) on two generic image datasets. For fair comparisons, the backbone of these methods in this table is CNN-F. Best results are marked in bold.

Datasets	# bits	ITQ	SDH	DPSH	HashNet	ADSH	CSQ	OrthoCos+BN	A ² -NET	A ² -NET ⁺⁺
NUS-WIDE	12	71.43	76.46	79.41	76.20	84.00	77.64	76.85	82.95	84.93
	24	73.61	79.98	82.49	78.54	87.84	78.92	79.64	87.57	88.90
	32	74.57	80.17	83.51	79.31	89.51	80.29	81.37	88.13	89.87
	48	75.53	81.24	84.42	79.76	90.55	80.52	82.01	89.43	90.68
COCO	12	63.38	69.54	74.61	76.49	83.88	79.40	76.00	86.42	87.84
	24	63.26	70.78	76.67	77.85	85.90	80.84	78.63	88.14	88.76
	32	63.08	71.15	77.29	78.38	86.33	82.16	80.35	88.97	89.91
	48	63.38	71.64	77.77	79.17	86.51	82.26	81.60	89.28	90.27

Table 4

Results in terms of retrieval accuracy (% mAP) with the zero-shot retrieval protocol [68] on three fine-grained datasets. For fair comparisons, the backbone of these methods in this table is ResNet-50. Best results are marked in bold.

Datasets	# bits	HashNet	ADSH	CSQ	OrthoCos+BN	ExchNet	A ² -NET	A ² -NET ⁺⁺
CUB200-2011	12	13.02	22.41	20.41	23.30	23.53	23.71	23.89
	24	22.58	39.02	31.51	38.82	39.51	39.67	41.32
	32	32.45	46.98	41.55	46.30	48.13	51.33	52.75
	48	42.02	52.91	48.32	51.89	53.77	58.47	62.71
Aircraft	12	16.54	21.84	22.34	22.14	23.03	23.45	24.14
	24	32.72	45.16	43.85	44.93	47.90	51.62	53.87
	32	39.44	50.95	49.49	49.38	53.22	58.91	60.38
	48	39.75	55.31	51.66	53.49	56.01	59.63	61.59
Food101	12	17.89	22.89	23.54	23.18	24.69	26.32	27.98
	24	36.54	42.65	41.74	42.01	43.11	45.25	47.85
	32	41.06	46.98	46.63	46.10	48.25	52.74	53.27
	48	41.85	50.31	47.72	50.69	51.87	55.97	56.30

Table 5

Results in terms of retrieval accuracy (% mAP) within cross-domain scenarios on the *Clothing* dataset [10]. For fair comparisons, the backbone of these methods in this table is ResNet-50. Best results are marked in bold.

Datasets	# bits	ITQ	SDH	DPSH	HashNet	ADSH	ExchNet	A ² -NET	A ² -NET ⁺⁺
Clothing	12	32.18	32.67	32.03	34.06	34.82	36.38	37.71	38.00
	24	32.25	33.39	32.87	33.84	35.64	37.06	38.11	38.98
	32	33.08	33.54	33.22	34.44	36.08	37.73	38.43	39.14
	48	33.91	34.32	34.15	34.51	36.33	38.24	39.04	39.33

the results of four hash bits with varying lengths, *i.e.*, 12, 24, 32, and 48, for evaluation. As shown in the table, our proposed A²-NET and A²-NET⁺⁺ models consistently outperform the other baseline methods on these datasets significantly. In particular, compared with the state-of-the-art method ExchNet [8], our A²-NET (A²-NET⁺⁺) achieves 17.83% (27.62%) and 17.88% (26.53%) improvements over ExchNet of 24-bit and 32-bit experiments on *Aircraft* and *Food-101*, respectively. Moreover, A²-NET also obtains superior results with an absolute value of about 80% mAP on *CUB200-2011*, *Aircraft* and *Food101* with 48-bit hash codes. While A²-NET⁺⁺ achieves much better results over A²-NET thanks to its simple but effective self-consistency enhancement, cf. Section 3.4.2. These observations validate the effectiveness of our models, as well as their promising practicality in real-world applications of fine-grained retrieval. Additionally, in Figure 6, we illustrate several retrieval results of A²-NET⁺⁺ on these fine-grained datasets, which shows that it can retrieve well among multiple subordinate categories when the same species of visual objects with diverse variations appear in different kinds of background. Also, there exist several failure cases, due to extremely subtle visual differences (*e.g.*,

caused by different views) between the query image and the returned images.

4.3.2 Comparisons on Generic Image Datasets

To further investigate the effectiveness and universality of our models, we conduct experiments on two generic image retrieval datasets, *i.e.*, *NUS-WIDE* and *COCO*. Except these classical and competitive baseline methods, we also compare with two recent state-of-the-arts in the field of generic hashing, *i.e.*, CSQ [44] and OrthoCos+BN [45]. As reported in Table 3, our A²-NET achieves comparable or slightly better results over strong baselines, including ADSH, CSQ and OrthoCos+BN. While, our A²-NET⁺⁺ consistently outperforms all methods by a large margin. The results prove that our models can also handle generic image hashing tasks well, rather than being limited to fine-grained hashing tasks.

4.3.3 Results of Zero-Shot Fine-Grained Retrieval

In the aforementioned experiments, we follow the traditional supervised hashing protocol, *i.e.*, supervised retrieval protocol where queries and database have identical classes [65], [68]. In order to further investigate the generalization ability

Table 6

Time and space complexity comparisons with baseline methods. Our A²-NET and A²-NET⁺⁺ models exhibit similar computational complexity during inference. “↑” (“↓”) denotes that the higher (lower) the better.

Methods	WCtime (↓)	Speedup (↑)	Memory (↓)
Linear	9481.03	1×	207.2MB
BallTree [69]	236.23	40.13×	28.1MB
KDTree [70]	70.16	135.13×	28.8MB
PQ [71]	43.49	217.99×	524.5KB
Ours	39.42	240.50×	380.2KB

of our models, the challenging zero-shot retrieval protocol [68] is also deployed, where queries and database have *different classes*. We compare several representative methods of both fine-grained hashing and generic hashing, and report the results on three fine-grained datasets in Table 4. As shown, our proposed models are still the optimal solution under the zero-shot retrieval setting, especially for A²-NET⁺⁺. Its retrieval accuracy is consistently and significantly better than other competing methods.

4.3.4 Results of Cross-Domain Fine-Grained Retrieval

Cross-domain fine-grained retrieval is a practical task for many real-world applications, *e.g.*, mobile product image search [10]. In experiments, we also consider such a protocol to test the robustness of our proposed models. In this concrete case, we employ the *Clothing* dataset [10] for retrieval accuracy evaluation. The corresponding empirical results are presented in Table 5. Similar observations are obtained with those ones in Table 2, where our proposed A²-NET and A²-NET⁺⁺ models significantly outperform other methods in the cross-domain fine-grained retrieval setting. It also reveals that our models could perform well in various practical scenarios with good potential. Also, we show the retrieval results of the *Clothing* dataset in Figure 6f for qualitative demonstration.

4.3.5 Time and Space Complexity During Inference

Retrieval efficiency plays a vital role in fine-grained hashing. To evaluate the efficiency of our models, we compare them with baseline approaches for approximate nearest neighbor (ANN) search, including two tree-based ANN approaches (*i.e.*, BallTree [69] and KDTree [70]) and one product quantization based ANN approach (*i.e.*, Product Quantization, PQ [71]). These baselines serve as references to assess the performance of our models in terms of wall clock time (WCtime), speedup ratio, and memory cost. In Table 6, we present the results of these comparisons. Our models demonstrate superior performance, achieving the lowest WCtime, highest speedup, and smallest memory cost when compared to the baseline ANN approaches. Notably, our models exhibit a remarkable query speedup of approximately 240 times.

4.4 Ablation Studies

In this section, we demonstrate the effectiveness of the crucial components of the proposed A²-NET⁺⁺ model, *i.e.*, the attention-based fine-grained representation learning component (*aka* “attention”, cf. Section 3.2), the unsupervised attribute-guided reconstruction component (*aka* “feature

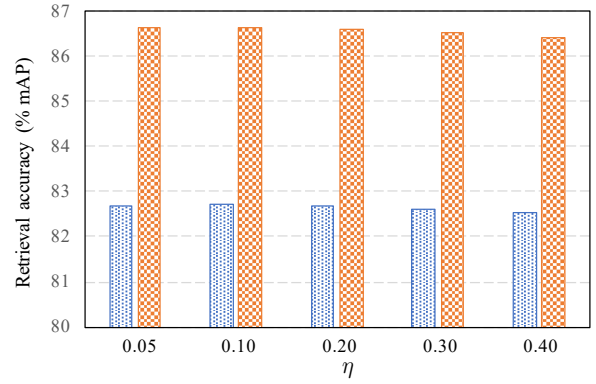


Figure 7. Comparisons of retrieval accuracy (% mAP) of different values of η , cf. Eq. (15). The blue bars represent the results for the *CUB200-2011* dataset, while the orange bars represent the results for the *Aircraft* dataset. All results are based on 48-bit hash codes.

reconstruction”, cf. Section 3.3.1), the self-consistent image reconstruction component (*aka* “image reconstruction”, cf. Section 3.4.2) and the attribute-specific feature decorrelation component (*aka* “feature decorrelation”, cf. Section 3.3.2). In the ablation studies, we apply these components incrementally on a vanilla backbone (*i.e.*, ResNet-50). As evaluated in Table 7, by stacking these components one by one, the retrieval results are steadily improved, which justifies the effectiveness of our proposed components in A²-NET⁺⁺. Besides, the results of A²-NET are presented as well, which can be compared with the results of the “+ Image reconstruction” column for clearly observing the large accuracy improvement derived from our novel self-consistency enhancement in Section 3.4.2 over the basic A²-NET model. Furthermore, we also provide more sufficient results of three variants of “+ Image reconstruction”, *i.e.*, reconstruction with only $\mathcal{I}_i^{g_i}$, with only $\mathcal{I}_i^{g_i}$ and with both $\mathcal{I}_i^{g_i} / \mathcal{I}_i^{g_i}$. It is clear to see that, reconstruction with only $\mathcal{I}_i^{g_i}$ brings slightly improvements, and reconstruction with only $\mathcal{I}_i^{g_i}$ improves the retrieval accuracy by a large margin. Reconstruction with both $\mathcal{I}_i^{g_i} / \mathcal{I}_i^{g_i}$ achieves further improvements over only $\mathcal{I}_i^{g_i}$ or $\mathcal{I}_i^{g_i}$, which not only verifies the proposed dual reconstruction is necessary, but also reveals that overcoming simplicity bias by our proposed self-consistent image reconstruction module significantly benefits fine-grained retrieval tasks.

In addition, the final learning objective of our A²-NET⁺⁺ model has four hyper-parameters, including λ , α , β , and η , cf. Eq. (15). Thanks to the robustness of our model, λ is fixed to 1 for all experiments, and α / β can be set according to the number of hash bits.¹ Regarding η , we hereby change its values of {0.05, 0.10, 0.20, 0.30, 0.40} for parameter analyses. As depicted in Figure 7, minimal variations can be observed across different values of η . This finding indicates that our model is not sensitive to parameter changes, highlighting its practical potential.

1. In the implementation details (cf. Section 4.2.2), α and β are set to $\frac{1}{n \times k}$ and $\frac{12}{k}$, respectively, where n is the number of training data in a batch and k is the number of hash bits.

Table 7

Retrieval accuracy (% mAP) with incremental components of the proposed A²-NET⁺⁺ model. The results of A²-NET⁺⁺ are reported in the penultimate column. We also present A²-NET’s results in the last column for clearly comparisons. Note that, the “+ Image reconstruction” column has three variants of equal status. Best results are marked in bold.

Datasets	# bits	Vanilla	+ Attention	+ Feature	+ Image	+ Image	+ Image	+ Feature	A ² -NET
		Backbone (ResNet-50)	(Sec. 3.2)	reconstruction (Sec. 3.3.1)	reconstruction (only $\mathcal{I}_i^{g_i}$ in Sec. 3.4.2)	reconstruction (only $\mathcal{I}_i^{g_i}$ in Sec. 3.4.2)	reconstruction (both $\mathcal{I}_i^{g_i} / \mathcal{I}_i^{g_i}$ in Sec. 3.4.2)	decorrelation (Sec. 3.3.2)	
CUB200-2011	12	20.03	27.42	33.31	33.42	34.27	36.13	37.83	33.83
	24	50.33	58.17	60.65	60.69	63.15	67.73	71.73	61.01
	32	61.68	68.24	71.28	71.36	74.63	77.67	78.39	71.61
	48	65.43	76.10	77.10	77.15	79.54	81.83	82.71	77.33
Aircraft	12	15.54	39.78	41.54	41.72	54.67	52.06	57.53	40.00
	24	23.09	61.73	64.47	64.60	66.24	70.63	73.45	63.66
	32	30.37	69.34	71.09	71.18	75.49	79.60	81.59	72.51
	48	50.65	79.21	81.14	81.22	82.93	84.52	86.65	81.37
Food101	12	35.64	41.33	45.02	45.63	47.50	50.67	54.51	46.44
	24	40.93	65.07	67.49	68.04	70.21	74.64	81.46	66.87
	32	42.89	70.06	73.57	73.74	74.51	75.73	82.92	74.27
	48	48.81	78.51	81.63	81.74	82.33	82.70	83.66	82.13
NABirds	12	2.34	5.03	7.91	7.93	8.13	8.46	8.80	8.20
	24	8.23	16.31	18.55	18.71	20.09	21.32	22.65	19.15
	32	14.71	22.34	23.87	23.96	26.88	28.14	29.79	24.41
	48	25.34	33.47	34.93	35.10	36.65	40.04	42.94	35.64
VegFru	12	8.24	22.14	24.79	24.98	26.43	27.86	30.54	25.52
	24	24.90	39.69	44.21	44.76	51.07	55.83	60.56	44.73
	32	36.53	47.08	51.04	51.80	63.41	67.98	73.38	52.75
	48	55.15	66.47	68.63	69.25	74.68	77.80	82.80	69.77

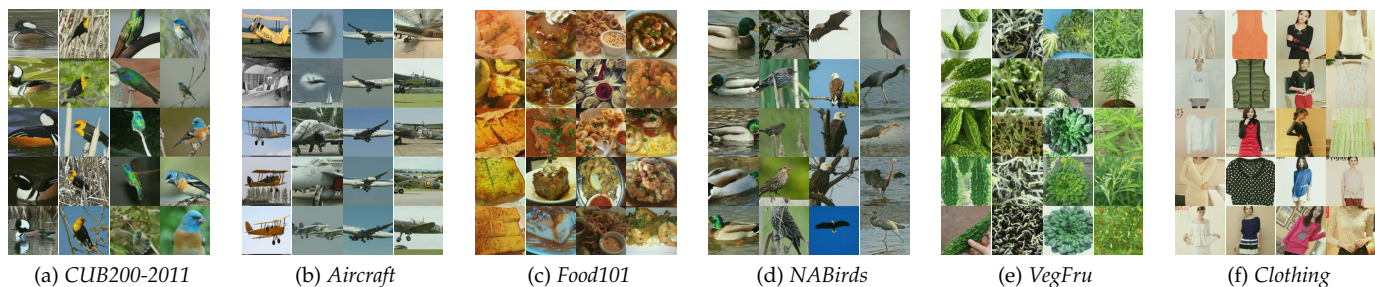


Figure 8. Quality demonstrations of the learned attribute-aware hash codes by the proposed A²-NET⁺⁺ model. Each column in each sub-figure can strongly correspond to a certain kind of properties of the fine-grained objects, e.g., “birds with black and white head in water”, “double-winged aircrafts”, “lumpy food”, “vegetables with uneven surfaces”, “lace clothing”, etc. (Best viewed in color and zoomed in.)

4.5 Attribute-Aware Retrieval Evaluation

As an important characteristic of our models, we hereby focus on the attribute-aware retrieval evaluation from both qualitative and quantitative perspectives.

4.5.1 Qualitative Analyses of Attribute-Aware Hash Codes

We firstly discuss the quality of the learned attribute-aware hash codes u_i of A²-NET⁺⁺. After obtaining u_i , we visualize fine-grained images retrieved by a random single hash bit of u_i to demonstrate the strong correspondence between visual attributes and the obtained hash bits. All the six datasets (also including *Clothing*) in experiments are used as examples to illustrate the quality. As observed in Figure 8, images of each column have some similar fine-grained object properties, i.e., visual attributes. Indeed, the learned hash codes are apparently attribute-aware, which could provide an explanation of the A²-NET⁺⁺’s success in fine-grained retrieval. Meanwhile, it also offers human-understandable interpretation for such a deep learning based fine-grained hashing method. Moreover, our A²-NET has similar characteristics of attribute awareness [24].

Table 8

Results in terms of NDCG@20 for evaluating the attribute-level matching on the *Clothing* dataset. Best results are marked in bold.

Methods	NDCG@20
ITQ	0.296
SDH	0.308
DPSH	0.319
HashNet	0.337
ADSH	0.342
ExchNet	0.374
A²-NET	0.396
A²-NET⁺⁺	0.405

4.5.2 Quantitative Results of Attribute Matching

Regarding the quantitative evaluation of our attribute-aware hash codes, we calculate the Normalized Discounted Cumulative Grain (NDCG@ k) metric [10] by performing our models on the *Clothing* dataset. Specifically, NDCG@ k equals to $\frac{1}{Z} \sum_{j=1}^k \frac{2^{rel(j)} - 1}{\log(j+1)}$, where $rel(j)$ is the relevance score of the j -th ranked image, and Z is a normalization constant. The relevance score $rel(j)$ of query image and the j -th ranked image is the number of their matched attributes divided by

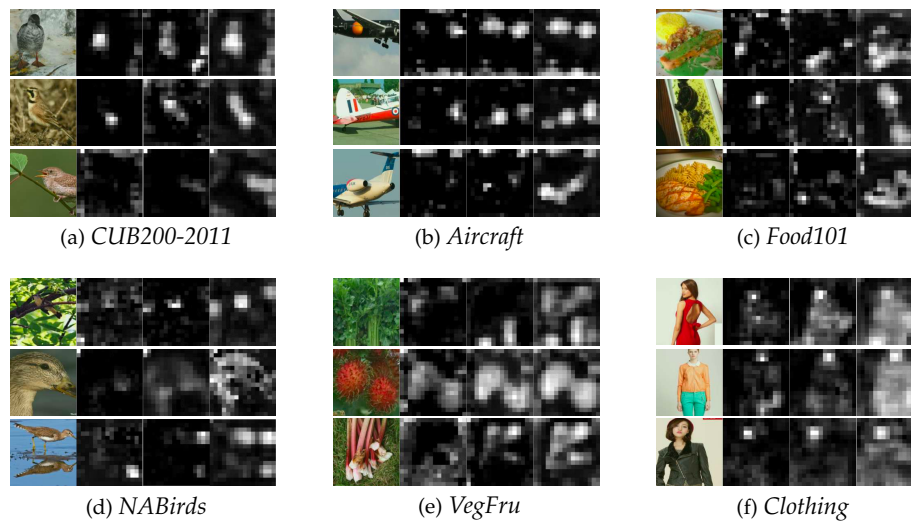


Figure 9. Input images and the corresponding activations. In each subfigure, the first column is the input image. The second column presents the activations of ExchNet. The third and fourth columns are the activations of our A^2 -NET and A^2 -NET $^{++}$.

the total number of query attributes. The detailed evaluation results in terms of NDCG@20 are reported in Table 8, where our models achieve the best score w.r.t strong attribute-level matching. It can quantitatively prove that our learned hash codes contains more similar attributes to the queries, as well as having strong explicit semantic meaning.

4.6 Visualization of Simplicity Bias on Fine-Grained Retrieval Datasets

Except for the activations on the *MNIST-CIFAR* dataset shown in Figure 4, we further visualize the activations on six fine-grained datasets (also including *Clothing*). As presented in Figure 9, we list the original input images and compare the corresponding activations of ExchNet [8] and our models. It is apparent to observe that although ExchNet obtains relatively good quantitative retrieval results of fine-grained hashing (cf. Table 2), its activations concentrate on some image regions corresponding to simple patterns but overlooking complex ones, which suggests that it still suffers from the pitfall of simplicity bias [15], [52]. In contrast, thanks to the self-consistency nature of the feature reconstruction process in our A^2 -NET, it focuses on more (meaningful) image regions corresponding to complex patterns than ExchNet. This enables A^2 -NET to learn more comprehensive fine-grained patterns and then to learn more discriminative binary hash codes for fine-grained hashing. Regarding A^2 -NET $^{++}$, further enhancing self-consistency by equipping image reconstruction makes it perform much better than A^2 -NET. In Figure 9, we can see that basically *all* object information has been completely attended, especially without ignoring the complex patterns, *e.g.*, textures of bird’s head, special painting of aircrafts’ fuselage, etc.

5 CONCLUSION

In this paper, we proposed attribute-aware hashing networks with self-consistency for dealing with the large-scale fine-grained image retrieval task. Particularly, our models were designed as expected to be efficient, effective and more

importantly interpretable. Concretely, by developing an unsupervised attribute-guided reconstruction method based on the obtained appearance-specific visual representation with attention, it can distill attribute-specific vectors in a high-level attribute space. After further performing feature decorrelation upon attribute-specific vectors, their discriminative ability is strengthened for representing a fine-grained object. Then, hash codes can be generated from these attribute-specific vectors and thus became attribute-aware. Through validation experiments of simplicity bias in deep hashing, we considered the model design from the perspective of the self-consistency principle and further enhanced model’s self-consistency by equipping an additional image reconstruction path. Both qualitative and quantitative experiments of various datasets and settings justified the superior of our models from different aspects in terms of effectiveness, robustness, generalization ability, interpretation, etc. Furthermore, visual attributes have been shown to be useful in describing visual entities, which motivates us to study identifying both fine-grained and generic categories under challenging scenarios, *e.g.*, novel class discovery, or weakly-supervised categorization/detection, based on our attribute-aware mechanism as the future work.

ACKNOWLEDGMENT

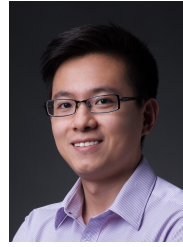
The authors would like to thank the editor and the anonymous reviewers for their critical and constructive comments and suggestions. We gratefully acknowledge the support of MindSpore, CANN (Compute Architecture for Neural Networks) and Ascend AI Processor used for this research.

REFERENCES

- [1] X.-S. Wei, Y.-Z. Song, O. M. Aodha, J. Wu, Y. Peng, J. Tang, J. Yang, and S. Belongie, “Fine-grained image analysis with deep learning: A survey,” *IEEE Trans. Pattern Anal. Mach. Intell.*, vol. 44, no. 12, pp. 8927–8948, 2022.
- [2] G. Van Horn, O. Mac Aodha, Y. Song, Y. Cui, C. Sun, A. Shepard, H. Adam, P. Perona, and S. Belongie, “The iNaturalist species classification and detection dataset,” in *Proc. IEEE Conf. Comp. Vis. Patt. Recogn.*, 2017, pp. 8769–8778.

- [3] J. Krause, M. Stark, J. Deng, and L. Fei-Fei, "3D object representations for fine-grained categorization," in *ICCV Workshop on 3D Representation and Recognition*, 2013.
- [4] X.-S. Wei, Q. Cui, L. Yang, P. Wang, L. Liu, and J. Yang, "RPC: A large-scale and fine-grained retail product checkout dataset," *SCIENCE CHINA Information Sciences*, vol. 65, no. 9, p. 197101, 2022.
- [5] T. Berg, J. Liu, S. W. Lee, M. L. Alexander, D. W. Jacobs, and P. N. Belhumeur, "Birdsnap: Large-scale fine-grained visual categorization of birds," in *Proc. IEEE Conf. Comp. Vis. Patt. Recogn.*, 2014, pp. 2019–2026.
- [6] Z. Liu, P. Luo, S. Qiu, X. Wang, and X. Tang, "DeepFashion: Powering robust clothes recognition and retrieval with rich annotations," in *Proc. IEEE Conf. Comp. Vis. Patt. Recogn.*, 2016, pp. 1096–1104.
- [7] S. Hou, Y. Feng, and Z. Wang, "VegFru: A domain-specific dataset for fine-grained visual categorization," in *Proc. IEEE Int. Conf. Comp. Vis.*, 2017, pp. 541–549.
- [8] Q. Cui, Q.-Y. Jiang, X.-S. Wei, W.-J. Li, and O. Yoshie, "ExchNet: A unified hashing network for large-scale fine-grained image retrieval," in *Proc. Eur. Conf. Comp. Vis.*, 2020, pp. 189–205.
- [9] S. Jin, H. Yao, X. Sun, S. Zhou, L. Zhang, and X. Hua, "Deep saliency hashing for fine-grained retrieval," *IEEE Trans. Image Process.*, vol. 29, pp. 5336–5351, 2020.
- [10] J. Huang, R. Feris, Q. Chen, and S. Yan, "Cross-domain image retrieval with a dual attribute-aware ranking network," in *Proc. IEEE Int. Conf. Comp. Vis.*, 2015, pp. 1062–1070.
- [11] N. Kumar, A. Berg, P. N. Belhumeur, and S. Nayar, "Describable visual attributes for face verification and image search," *IEEE Trans. Pattern Anal. Mach. Intell.*, vol. 33, no. 10, pp. 1962–1977, 2011.
- [12] H. Zhang, X. Cao, and R. Wang, "Audio visual attribute discovery for fine-grained object recognition," in *Proc. Conf. AAAI*, 2018, pp. 7542–7549.
- [13] Y. Xian, C. H. Lampert, B. Schiele, and Z. Akata, "Zero-shot learning—a comprehensive evaluation of the good, the bad and the ugly," *IEEE Trans. Pattern Anal. Mach. Intell.*, vol. 41, no. 9, pp. 2251–2265, 2019.
- [14] Y. Ma, D. Tsao, and H.-Y. Shum, "On the principles of parsimony and self-consistency for the emergence of intelligence," *Frontiers of Information Technology and Electronic Engineering*, vol. 23, no. 9, pp. 1298–1323, 2022.
- [15] H. Shah, K. Tamuly, A. Raghunathan, P. Jain, and P. Netrapalli, "The pitfalls of simplicity bias in neural networks," in *Advances in Neural Inf. Process. Syst.*, 2020, pp. 9573–9585.
- [16] D. C. Ciresan, U. Meier, J. Masci, L. M. Gambardella, and J. Schmidhuber, "High-performance neural networks for visual object classification," *arXiv preprint arXiv:1102.0183*, pp. 1–12, 2011.
- [17] A. Krizhevsky and G. Hinton, "Learning multiple layers of features from tiny images," *Citeseer*, Tech. Rep., 2009.
- [18] C. Wah, S. Branson, P. Welinder, P. Perona, and S. Belongie, "The Caltech-UCSD birds-200-2011 dataset," *Tech. Report CNS-TR-2011-001*, 2011.
- [19] S. Maji, E. Rahtu, J. Kannala, M. Blaschko, and A. Vedaldi, "Fine-grained visual classification of aircraft," *arXiv preprint arXiv:1306.5151*, 2013.
- [20] L. Bossard, M. Guillaumin, and L. V. Gool, "Food-101 – mining discriminative components with random forests," in *Proc. Eur. Conf. Comp. Vis.*, 2014, pp. 446–461.
- [21] G. Van Horn, S. Branson, R. Farrell, S. Haber, J. Barry, P. Ipeirotis, P. Perona, and S. Belongie, "Building a bird recognition app and large scale dataset with citizen scientists: The fine print in fine-grained dataset collection," in *Proc. IEEE Conf. Comp. Vis. Patt. Recogn.*, 2015, pp. 595–604.
- [22] T.-S. Chua, J. Tang, R. Hong, H. Li, Z. Luo, and Y. Zheng, "NUS-WIDE: A real-world web image database from National University of Singapore," in *Proc. ACM Int. Conf. on Image and Video Retrieval*, 2009, pp. 1–9.
- [23] T.-Y. Lin, M. Maire, S. Belongie, J. Hays, P. Perona, D. Ramanan, and P. D. and C. Lawrence Zitnick, "Microsoft COCO: Common objects in context," in *Proc. Eur. Conf. Comp. Vis.*, 2014, pp. 740–755.
- [24] X.-S. Wei, Y. Shen, X. Sun, H.-J. Ye, and J. Yang, "A²-Net: Learning attribute-aware hash codes for large-scale fine-grained image retrieval," in *Advances in Neural Inf. Process. Syst.*, 2021, pp. 5720–5730.
- [25] X.-S. Wei, J.-H. Luo, J. Wu, and Z.-H. Zhou, "Selective convolutional descriptor aggregation for fine-grained image retrieval," *IEEE Trans. Image Process.*, vol. 26, no. 6, pp. 2868–2881, 2017.
- [26] X. Zheng, R. Ji, X. Sun, Y. Wu, F. Huang, and Y. Yang, "Centralized ranking loss with weakly supervised localization for fine-grained object retrieval," in *Proc. Int. Joint Conf. Artificial Intell.*, 2018, pp. 1226–1233.
- [27] X. Zheng, R. Ji, X. Sun, B. Zhang, Y. Wu, and F. Huang, "Towards optimal fine grained retrieval via decorrelated centralized loss with normalize-scale layer," in *Proc. Conf. AAAI*, 2019, pp. 9291–9298.
- [28] Y. Li, T. M. Hospedales, Y.-Z. Song, and S. Gong, "Fine-grained sketch-based image retrieval by matching deformable part models," in *Proc. British Machine Vis. Conf.*, 2014, pp. 1–12.
- [29] Q. Yu, F. Liu, Y.-Z. Song, T. Xiang, T. M. Hospedales, and C.-C. Loy, "Sketch me that shoe," in *Proc. IEEE Conf. Comp. Vis. Patt. Recogn.*, 2016, pp. 799–807.
- [30] K. Pang, Y. Yang, T. M. Hospedales, T. Xiang, and Y.-Z. Song, "Solving mixed-modal jigsaw puzzle for fine-grained sketch-based image retrieval," in *Proc. IEEE Conf. Comp. Vis. Patt. Recogn.*, 2020, pp. 10347–10355.
- [31] X. Zeng, Y. Zhang, X. Wang, K. Chen, D. Li, and W. Yang, "Fine-grained image retrieval via piecewise cross entropy loss," *Image and Vision Computing*, vol. 93, pp. 2868–2881, 2020.
- [32] J. Zhang, F. Shen, L. Liu, F. Zhu, M. Yu, L. Shao, H. Tao Shen, and L. Van Gool, "Generative domain-migration hashing for sketch-to-image retrieval," in *Proc. Eur. Conf. Comp. Vis.*, 2018, pp. 297–314.
- [33] K. Li, K. Pang, Y.-Z. Song, T. M. Hospedales, T. Xiang, and H. Zhang, "Synergistic instance-level subspace alignment for fine-grained sketch-based image retrieval," *IEEE Trans. Image Process.*, vol. 26, no. 12, pp. 5908–5921, 2017.
- [34] J. Bromley, I. Guyon, Y. LeCun, E. Säckinger, and R. Shah, "Signature verification using a "siamese" time delay neural network," in *Advances in Neural Inf. Process. Syst.*, 1993, pp. 737–744.
- [35] T. Chen, S. Kornblith, M. Norouzi, and G. Hinton, "A simple framework for contrastive learning of visual representations," in *Proc. Int. Conf. Mach. Learn.*, 2020, pp. 1597–1607.
- [36] M. Corbetta and G. L. Shulman, "Control of goal-directed and stimulus-driven attention in the brain," *Nature Reviews Neuroscience*, vol. 3, pp. 201–215, 2002.
- [37] A. Sain, A. K. Bhunia, Y. Yang, T. Xiang, and Y.-Z. Song, "Cross-modal hierarchical modelling for fine-grained sketch based image retrieval," in *Proc. British Machine Vis. Conf.*, 2020, pp. 1–14.
- [38] S. Jin, H. Yao, X. Sun, S. Zhou, L. Zhang, and X. Hua, "Deep saliency hashing for fine-grained retrieval," *IEEE Trans. Image Process.*, vol. 29, pp. 5336–5351, 2020.
- [39] Z.-D. Chen, X. Luo, Y. Wang, S. Guo, and X.-S. Xu, "Fine-grained hashing with double filtering," *IEEE Trans. Image Process.*, vol. 31, pp. 1671–1683, 2022.
- [40] J. Wang, H. T. Shen, and T. Zhang, "A survey on learning to hash," *IEEE Trans. Pattern Anal. Mach. Intell.*, vol. 40, no. 4, pp. 769–790, 2018.
- [41] A. Dasgupta, R. Kumar, and T. Sarlos, "Fast locality-sensitive hashing," in *Proc. ACM SIGKDD Int. Conf. Knowledge Discovery & Data Mining*, 2011, pp. 1073–1081.
- [42] Q. Lv, W. Josephson, Z. Wang, M. Charikar, and K. Li, "Multi-probe LSH: Efficient indexing for high-dimensional similarity search," in *Proc. Int. Conf. Very Large Data Bases*, 2007, pp. 950–961.
- [43] A. Shrivastava and P. Li, "Densifying one permutation hashing via rotation for fast near neighbor search," in *Proc. Int. Conf. Mach. Learn.*, 2014, pp. 557–565.
- [44] L. Yuan, T. Wang, X. Zhang, F. E. Tay, Z. Jie, W. Liu, and J. Feng, "Central similarity quantization for efficient image and video retrieval," in *Proc. IEEE Conf. Comp. Vis. Patt. Recogn.*, 2020, pp. 3083–3092.
- [45] J. T. Hoe, K. W. Ng, T. Zhang, C. S. Chan, Y.-Z. Song, and T. Xiang, "One loss for all: Deep hashing with a single cosine similarity based learning objective," in *Advances in Neural Inf. Process. Syst.*, 2021, pp. 24286–24298.
- [46] Q.-Y. Jiang and W.-J. Li, "Asymmetric deep supervised hashing," in *Proc. Conf. AAAI*, 2018, pp. 3342–3349.
- [47] F. Shen, C. Shen, W. Liu, and H. T. Shen, "Supervised discrete hashing," in *Proc. IEEE Conf. Comp. Vis. Patt. Recogn.*, 2015, pp. 37–45.
- [48] F. Cakir, K. He, S. A. Bargal, and S. Sclaroff, "Hashing with mutual information," *IEEE Trans. Pattern Anal. Mach. Intell.*, vol. 41, no. 10, pp. 2424–2437, 2019.
- [49] K. He, F. Cakir, S. A. Bargal, and S. Sclaroff, "Hashing as tie-aware learning to rank," in *Proc. IEEE Conf. Comp. Vis. Patt. Recogn.*, 2018, pp. 4023–4032.
- [50] V. Ferrari and A. Zisserman, "Learning visual attributes," in *Advances in Neural Inf. Process. Syst.*, 2007, pp. 433–440.

- [51] G. Patterson, C. Xu, H. Su, and J. Hays, "The SUN attribute database: Beyond categories for deeper scene understanding," *Int. J. Comput. Vision*, vol. 108, no. 1-2, pp. 59–81, 2014.
- [52] M. Huh, H. Mobahi, R. Zhang, B. Cheung, P. Agrawal, and P. Isola, "The low-rank simplicity bias in deep networks," *arXiv preprint arXiv:2103.10427*, 2021.
- [53] D. Teney, E. Abbasnejad, S. Lucey, and A. van den Hengel, "Evading the simplicity bias: Training a diverse set of models discovers solutions with superior ood generalization," in *Proc. IEEE Conf. Comp. Vis. Patt. Recogn.*, 2022, pp. 16 761–16 772.
- [54] L. Itti, C. Koch, and E. Niebur, "A model of saliency-based visual attention for rapid scene analysis," *IEEE Trans. Pattern Anal. Mach. Intell.*, vol. 20, no. 11, pp. 1254–1259, 1998.
- [55] H. Larochelle and G. Hinton, "Learning to combine foveal glimpses with a third-order boltzmann machine," in *Advances in Neural Inf. Process. Syst.*, 2010, pp. 1243–1251.
- [56] M. Ranzato, Y.-L. Boureau, S. Chopra, and Y. LeCun, "A unified energy-based framework for unsupervised learning," in *Proc. Int. Conf. Artificial Intell. and Statistics*, 2007, pp. 371–379.
- [57] R. Shwartz-Ziv and N. Tishby, "Opening the black box of deep neural networks via information," *arXiv preprint arXiv:1703.00810*, 2017.
- [58] N. Tishby and N. Zaslavsky, "Deep learning and the information bottleneck principle," in *Proc. IEEE Infor. Theory Workshop*, 2015, pp. 1–5.
- [59] N. Tishby, F. Pereira, and W. Bialek, "The information bottleneck method," in *Proc. Annual Allerton Conference on Communication, Control and Computing*, 1999, pp. 368–377.
- [60] C. Guo, G. Pleiss, Y. Sun, and K. Q. Weinberger, "On calibration of modern neural networks," in *Proc. Int. Conf. Mach. Learn.*, 2017, pp. 1321–1330.
- [61] K. He, X. Zhang, S. Ren, and J. Sun, "Deep residual learning for image recognition," in *Proc. IEEE Conf. Comp. Vis. Patt. Recogn.*, 2016, pp. 770–778.
- [62] M. D. Zeiler, D. Krishnan, G. W. Taylor, and R. Fergus, "Deconvolutional networks," in *Proc. IEEE Conf. Comp. Vis. Patt. Recogn.*, 2010, pp. 2528–2535.
- [63] Y. Gong, S. Lazebnik, A. Gordo, and F. Perronnin, "Iterative quantization: A procrustean approach to learning binary codes for large-scale image retrieval," *IEEE Trans. Pattern Anal. Mach. Intell.*, vol. 35, no. 12, pp. 2916–2929, 2012.
- [64] W.-J. Li, S. Wang, and W.-C. Kang, "Feature learning based deep supervised hashing with pairwise labels," in *Proc. Int. Joint Conf. Artificial Intell.*, 2015, pp. 1711–1717.
- [65] Z. Cao, M. Long, J. Wang, and P. S. Yu, "HashNet: Deep learning to hash by continuation," in *Proc. IEEE Int. Conf. Comp. Vis.*, 2017, pp. 5608–5617.
- [66] K. Chatfield, K. Simonyan, A. Vedaldi, and A. Zisserman, "Return of the devil in the details: Delving deep into convolutional nets," in *Proc. British Machine Vis. Conf.*, 2014, pp. 1–11.
- [67] W.-J. Li, S. Wang, and W.-C. Kang, "Feature learning based deep supervised hashing with pairwise labels," in *Proc. Int. Joint Conf. Artificial Intell.*, 2016, pp. 1711–1717.
- [68] C. Ma, I. W. Tsang, F. Peng, and C. Liu, "Partial hash update via hamming subspace learning," *IEEE Trans. Image Process.*, vol. 26, no. 4, pp. 1939–1951, 2017.
- [69] T. Liu, A. W. Moore, and A. Gray, "New algorithms for efficient high-dimensional nonparametric classification," *J. Mach. Learn. Res.*, vol. 7, pp. 1135–1158, 2006.
- [70] J. L. Bentley, "Multidimensional binary search trees used for associative searching," *Communications of the ACM*, vol. 18, no. 9, pp. 509–517, 1975.
- [71] H. Jégou, M. Douze, and C. Schmid, "Product quantization for nearest neighbor search," *IEEE Trans. Pattern Anal. Mach. Intell.*, vol. 33, no. 1, pp. 117–128, 2011.



Xiu-Shen Wei is a Professor with the School of Computer Science and Engineering, Southeast University, China. He was a Program Chair for the workshops associated with ICCV, IJCAI, ACM Multimedia, etc. He has also served as an Area Chair or Senior Program Member at CVPR, AAAI, IJCAI, ICME, BMVC, a Guest Editor of Pattern Recognition Journal, and a Tutorial Chair for Asian Conference on Computer Vision (ACCV) 2022.



Yang Shen is a Ph.D. Candidate under the supervision of Prof. Xiu-Shen Wei with School of Computer Science and Engineering, Nanjing University of Science and Technology, China. His research interests lie in deep learning and computer vision.



Xuhao Sun is a Master Student with School of Computer Science and Engineering, Nanjing University of Science and Technology, China. His main research interests are Computer Vision and Machine Learning.



Peng Wang is a Professor with School of Computer Science and Engineering, University of Electronic Science and Technology of China. He holds a PhD from School of Information Technology and Electrical Engineering at The University of Queensland. Dr. Peng Wang's primary research focus centers around computer vision and machine learning, with a particular emphasis on label-efficient deep learning techniques.



Yuxin Peng is currently the Boya Distinguished Professor with the Wangxuan Institute of Computer Technology, and National Key Laboratory for Multimedia Information Processing, Peking University. He received the Ph.D. degree in computer applied technology from Peking University in 2003. He has authored over 180 papers, including more than 90 papers in the top-tier journals and conference proceedings. He has submitted 48 patent applications and been granted 39 of them. His current research interests

mainly include cross-media analysis and reasoning, image and video recognition and understanding, and computer vision. He led his team to win the First Place in video instance search evaluation of TRECVID ten times in the recent years. He won the First Prize of the Beijing Technological Invention Award in 2016 (ranking first) and the First Prize of the Scientific and Technological Progress Award of Chinese Institute of Electronics in 2020 (ranking first). He was a recipient of the National Science Fund for Distinguished Young Scholars of China in 2019, and the best paper award at MMM 2019 and NCIG 2018. He serves as the associate editor of IEEE TMM, TCSVT, etc.